Theor Chim Acta (1992) 84: 195–215

Theoretica Chimica Acta

Structure and electron density distribution of the nitrate ion and urea molecule upon protonation

Guus J. M. Velders and Dirk Feil

Chemical Physics Laboratory, University of Twente, PO Box 217, NL-7500 AE Enschede, The Netherlands

Received March 9, 1992/Accepted April 21, 1992

Summary. The changes in the structure and electron density distribution of the nitrate ion and urea molecule upon the presence of a point charge are discussed. Analyses of the Cambridge Structural Database are performed as well as Hartree–Fock calculations on the appropriate molecules in the presence of a point charge. The Hartree–Fock calculations confirm the correlations in structural parameters found in the database. A charge analysis of the molecules explains part of the structural changes caused by the presence of the point charge. The electrostatic potential and Laplacian of the electron density distribution explain the position of the point charge relative to the molecules.

Key words: Hartree–Fock – Charge analysis – Electrostatic potential – Laplacian of charge density

1 Introduction

Most quantum chemical studies are concerned with properties of free atoms and molecules. Comparing calculated results with experiments is not straightforward, because molecules in liquids and solids are surrounded by neighbouring molecules. These neighbouring molecules influence the properties of the molecules under investigation. Intermolecular interactions and the resulting changes in molecular properties are an interesting field of research varying from solvation effects and intermolecular interaction potentials to chemical reaction mechanisms.

Quantum chemical calculations yield reasonable results for several molecular properties. Intermolecular interactions, on the other hand, are small and hard to calculate. Protonation of a molecule can be regarded as a process possessing features of molecular interactions and chemical reactions.

In this paper we will discuss quantum chemical calculations of the protonation of molecules, to obtain information about changes in molecular properties which will, to a smaller extent, also be present in more complex intermolecular interactions.

Besides quantum chemistry, there is also an experimental method for studying molecular interactions. The method makes use of crystallographic data and

is known as the structure-correlation method [1, 2]. The structure of a molecule in a crystal environment is not necessarily identical with the equilibrium structure of the isolated molecule, i.e. intermolecular forces exerted by the crystal environment deform a molecule to a certain extent. The structure of a molecular fragment will consequenlty not depend only on the constituting atoms, but also on the particular molecules of which it is a part, as well as on the crystal environment.

In the structure-correlation method deformations in molecular geometries are studied together with geometrical aspects of molecular packing. The method does not say anything about the intra- and intermolecular forces causing these deformations. As many structures as possible are collected, all containing the molecule or molecular fragment of interest. Each structure contains information about an experimental conformation of the molecular fragment. Different molecular environments will cause different deformations of a fragment. When in a large number of different crystals a specific fragment is present, the intrinsic properties of the fragment will be visible in the collection of structures. The source of the specific deformation is not important; the different molecular environments can be regarded as different perturbations acting on the fragment. These perturbations will in general be small compared to intramolecular forces.

An important application of the structure-correlation method is concerned with chemical reaction mechanisms. A structural fragment can be regarded as a point in a many-dimensional space, one dimension for each structural parameter. Different molecular environments yield different points in this configuration space. These points can be seen as intermediate states of a chemical reaction and are assumed to be a representation of the molecular potential energy hypersurface. The basic assumption behind the structure-correlation method is that a distribution of sample points corresponding to observed structures will tend to be concentrated in a low-lying region of the potential energy surface. This assumption is valid when environmental effects are small compared with intramolecular interactions.

The work described in this paper is based on both analysis of crystallographic data and on quantum chemical calculations. We are interested in the relations between bond lengths and bond angles in molecules present in crystal structures and try to interpret the relations by using electron densities distributions from quantum chemical calculations. The Cambridge Structural Database (CSD) [3] contains information of, at the moment, more than 90,000 organic crystal structures (version July 1991). We will discuss the correlations existing between bond lengths and angles of the nitrate ion (NO_3^-) and the molecular fragment N_2CO, as in the urea molecule. Both these structures are analyzed, as well as the same fragments with an extra covalent bond to an oxygen atom. This extra bond is caused by an atom which is within bonding distance of an atom of the fragment. The changes in the geometry of the fragments caused by the extra covalent bond are studied. The fragments NO_3 and N_2CO are present in a large number of structures of the CSD. Different atoms can form a bond with the oxygen atoms of these fragments.

In our quantum chemical calculations the different atoms, as well as different crystallographic environments, are represented by a single positive charge. This positive charge is in the calculations responsible for the extra bond with an oxygen atom. The magnitude and position of the charge are varied and the effects on the geometry of the fragments are studied. We performed Hartree–Fock calculations on the fragments with and without the presence of the point

charge. The geometries are compared with the crystallographic data while the electron density distributions of the fragments are analyzed to understand the molecular behaviour.

Adding a positive charge of $1|e|$ at an appropriate position is equivalent to protonation of molecules. Most quantum chemical studies of protonation are mainly concerned with the protonation energy and changes in the geometry upon protonation [4–7]. Umegama and Morokume [8] performed an energy decomposition of the energy of protonation and found that the polarizability of the molecules is important. Del Bene et al. [9–14] studied the influence of different substituent groups R on the protonation of R_2CO. They studied protonation energies, changes in molecular geometries and Mulliken population analysis.

The quantum chemical calculations of the protonation of molecules, presented here, are analyzed on basis of changes in the geometries, the topology of the electron density distribution and with the aid of the Hirshfeld charge partitioning method.

2 Methods

2.1 Structural data from the CSD

The CSD has been searched for the NO_3 and N_2CO fragments both with and without a single extra atom bonded to one of the oxygen atoms. Figure 1 shows these structures together with the definition of the bond lengths and angles. The searches have been performed using the programs QUEST [15] and GSTAT [16]. Besides the definition of the fragments, the following qualifiers have been used in the program GSTAT to select the structures:

- NERR — Exclude error entries.
- TIN 3 3 — Data collected with diffractometer.
- AVS 1 3 — Mean estimated standard deviations of C–C bond smaller than 0.030 Å.
- NDIS — Exclude disordered structures.
- NOD — Avoid duplicate of fragments.
- CHI 3 REJ — Rejection of outliers on the basis of a χ^2 analysis of the bond lengths and angles.

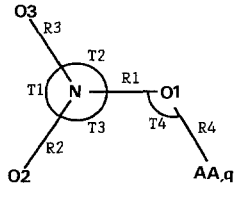

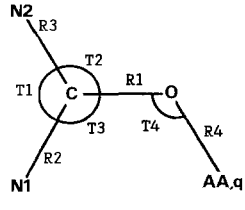

Fig. 1. Definition of the fragments. AA stands for Any Atom, q for a point charge. Flatness of the fragment: Q1 = dihedral angle N–O3–O2–O1. Extra atom relative to the fragment: Q2 = dihedral angle O2–N–O1–AA. The absolute values of Q1 and Q2 are always used. Similar definitions for the N_2CO–AA fragment

We used these restrictions to obtain a set of fragments with well determined structural parameters. Fragments with structural parameters deviating far from the average are considered to be outliers and rejected on basis of a χ^2 analysis. In a CSD search the covalent bonds are selected on the basis of standard covalent radii used in the programs. The definition of the NO_3 fragment does not allow extra atoms to be within bonding distance of the oxygen atoms, which would influence the geometry of the fragment.

Because the number of urea molecules and 'protonated' urea molecules in the CSD is small (18 respectively 13) we performed a search for N_2CO fragments, in which different types of atoms are allowed to be bonded to the nitrogen atoms. For the final statistics, the C–N bond is not allowed to form part of a cyclic bond. In this way we avoid the fragment to be part of a ring structure, since this will influence the geometry of the fragment considerably.

2.2 Quantum chemical methods

Restricted Hartree–Fock (HF) calculations [17, 18] are performed on the nitrate ion and the urea molecule to clarify the structural changes found in the fragments in the CSD. For most of the HF calculations a geometry optimization is performed in which all the bond lengths and angles are varied. Two basis sets are used for the calculations: 4-31G and 6-31G**.

Strong interactions between the fragments (NO_3 and N_2CO) and the environment are in the CSD analysis represented by an atom AA (= Any Atom), within bonding distance from an atom of the fragment. In the quantum chemical calculations this atom is replaced by a point charge q, of which the magnitude and position are varied. For the calculations atomic basis functions, corresponding to the basis set of a hydrogen atom, are placed on the point charge. The same basis set is used for all values of q. Placing no basis functions on the point charge causes the functions centred on the oxygen atom to describe the charge pulled in the direction of q. The flexibility of these functions determines to a large extent the position of q relative to the molecule. We have found for our calculations that reliable results can only be obtained when basis functions are placed on the point charge. The size of this basis set is not found to be very important.

2.3 Methods of analyses

The calculations are analyzed, apart from the changes in the geometries, by the electron density distributions $\varrho(r)$. For this purpose we make use of density maps, the Hirshfeld charge partitioning scheme (see Sect. 2.3.1) and the topological analysis of the electron density according to Bader's theory (see Sect. 2.3.2).

2.3.1 Hirshfeld's charge partitioning method. To obtain quantitative information from the electron density distribution atomic charges and multipole moments can be calculated. Since there is no unique way to define atomic charges several methods [19] are in use. Very popular from the quantum chemical point of view is the Mulliken [20, 21] partitioning method to analyze a LCAO-MO-SCF wavefunction. Unfortunately Mulliken atomic charges as well as the Löwdin [22] atomic charges are quite sensitive for the basis set used in the calculation.

The Hirshfeld [23] stockholder partitioning method is closely related to the definition of the promolecule, i.e. the sum of the electron density distributions of

the free spherical atoms constituting the molecule. In this formalism one defines for each atom a sharing function:

$$W_a(r) = \frac{\varrho_a^{\text{atom}}(r - R_a)}{\sum_b \varrho_b^{\text{atom}}(r - R_b)}, \tag{1}$$

where $\varrho_a^{\text{atom}}(r - R_a)$ is the spherically averaged free atomic density distribution of atom a at position R_a. The sum in the denominator runs over all atoms of the molecule. Using this sharing function the net atomic charges q_a and dipole moments μ_a are calculated from:

$$q_a = -\int W_a(r)\varrho(r)\, dr + Z_a \tag{2}$$

$$\mu_{ai} = -\int W_a(r)\varrho(r)(r_i - R_{ai})\, dr \tag{3}$$

with similar terms for higher order moments. (The nuclear charge is denoted by Z_a.) Since no analytic expression is available these terms have to be evaluated numerically using Gauss–Legendre quadrature. The advantage of this way of partitioning is that the atomic charges and multipole moments can be derived from any charge distribution, obtained by theory or experiment. Using this method in quantum chemical calculations, the atomic moments are far less sensitive for the basis set used in the calculation than those obtained with the methods from Mulliken and Löwdin.

2.3.2 Charge analysis according to Bader. The charge partitioning method discussed before lacks the profound quantum chemical basis present in the method proposed by Bader [24]. His method is based on the topology of the electron density distribution and defines an atom as the union of an attractor, the nucleus, and its associated basin:

$$\nabla\varrho(r) \cdot n(r) = 0, \quad \text{(for all points on the surface)} \tag{4}$$

where n is the vector normal to the surface of the atom. A nucleus acts as an attractor of the $\nabla\varrho(r)$ field; all the trajectories in some neighbourhood of a nucleus, its basin, terminate at the nucleus. The trajectories are lines of steepest ascent through the density distribution. A trajectory always stays within the basin in which it originates, i.e. Eq. (4) does not allow trajectories to cross the atomic surface which is therefore also referred to as a zero flux surface. The charge density is characterized by its extrema, or critical points, points at which the gradient vanishes, $\nabla\varrho(r) = 0$. Whether a critical point in $\varrho(r)$ is a maximum or a minimum is determined by the sign of the curvatures (second derivatives) of $\varrho(r)$. The trace of the Hessian matrix of $\varrho(r)$, the second derivative matrix, is called the Laplacian of $\varrho(r)$:

$$\nabla^2\varrho(r) = \left[\frac{\partial^2}{\partial x^2} + \frac{\partial^2}{\partial y^2} + \frac{\partial^2}{\partial z^2}\right]\varrho(r) \tag{5}$$

and is invariant to the choice of coordinate system. The principal axes and corresponding curvatures at the critical point are obtained as the eigenvectors and eigenvalues of the Hessian matrix. The rank of a critical point is denoted by ω and equals the number of non-zero eigenvalues of $\varrho(r)$ at the critical point. The signature σ is the algebraic sum of the signs of the eigenvalues of $\varrho(r)$ at the critical point. A critical point is labelled by the double (ω, σ) [24, 25].

Properties of the atoms defined by Eq. (4) can be calculated by performing the appropriate integrations [26, 27] over the atomic volumes and surfaces. Because of the complicated definition of the sharp boundary of the atom the calculation of atomic properties is rather complicated and computationally demanding.

Important for the position where a point charge will approach a molecule is the potential [28–30] surrounding the molecule. Bader [24, 31, 32] showed that the Laplacian $\nabla^2\varrho(r)$ contains similar information. Regions of space where $\nabla^2\varrho < 0$, charge is locally concentrated and a positive charge is most likely to approach a molecule at a local minimum in $\nabla^2\varrho$. Calculations of the potential and $\nabla^2\varrho$ are performed for the two molecules and the extrema of these quantities are determined. The relation between the molecular geometry and the positions and magnitudes of the extrema is discussed.

3 Results and discussion

3.1 Correlations in the CSD

3.1.1 The NO_3 fragments. In Tables 1 and 2 and in Fig. 2 the results of analysis of the CSD for the nitrate (NO_3 and NO_3–AA) fragments are shown. The following observations can be made from the tables, histograms and scatter diagrams comparing the NO_3 and NO_3–AA fragments.

The presence of the atom AA results in a larger bond length R1 (N–O1) in NO_3–AA than in NO_3 (Table 1), while the spread in this bond length in

Table 1. Geometry of nitrate fragments (NO_3 and NO_3–AA) from the CSD. Bond lengths in Å, angles in degrees. $\bar{x}$ is the average value and σ_x the standard deviation in the observed parameters. See Fig. 1 for the definition of the parameters

	NO_3[a]		NO_3–AA[b]	
	$\bar{x}$	σ_x[c]	$\bar{x}$	σ_x[c]
R1	1.231[d]	0.025	1.318	0.075
R2			1.215	0.024
R3			1.214	0.021
R4			1.974	0.425
T1	119.96[d]	2.15	124.66	4.34
T2			116.62	3.96
T3			118.69	1.61
T4			115.19	8.11
Q1[e]	0.03	2.21	0.32	1.40
Q2[e]			2.70	20.33

[a] The number of structures is 338
[b] The number of structures is 157
[c] Standard deviation in the observed parameters
[d] Average values of the three indistinguishable bond lengths/angles
[e] Q1 and Q2 can be both positive and negative here

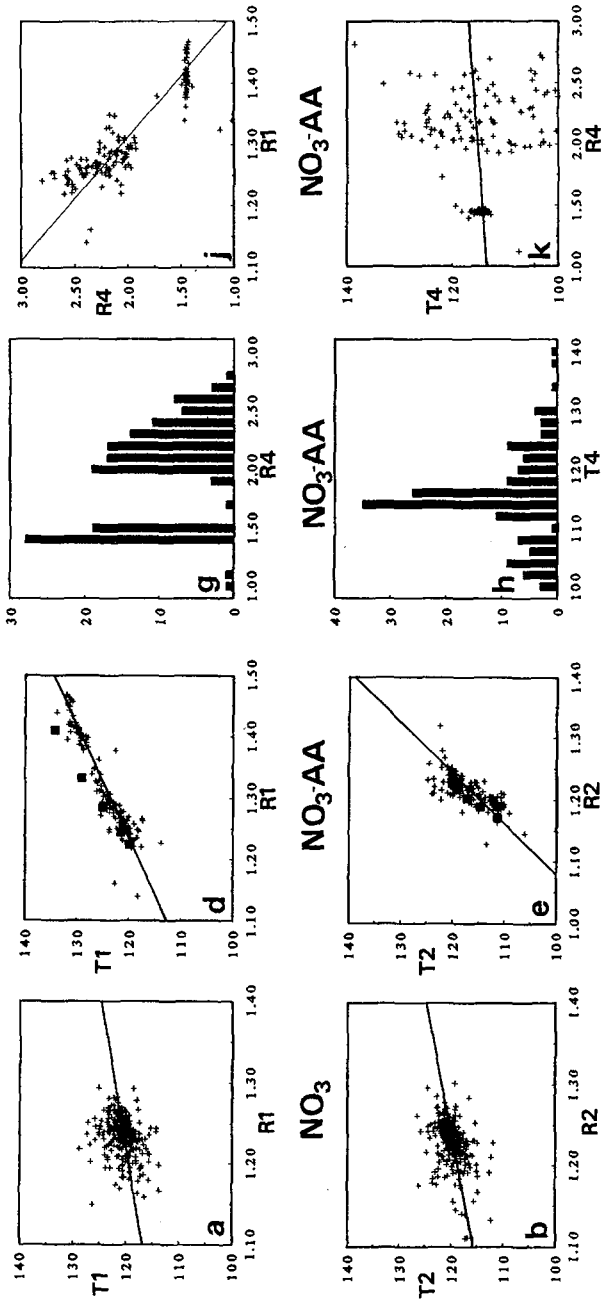

Fig. 2. Scatter diagrams and histograms of the NO_3 (*a–c*) and NO_3–AA (*d–l*) fragments. Each dot represents a structure in the CSD. The *straight line* represents a least squares fit with the data from the CSD. The *solid squares* represent the HF/6-31G** calculations

Table 2. Correlation matrices of the structural parameters of the NO_3 and NO_3–AA fragments

NO_3	R1	R2	R3	T1	T2	T3
R2	0.19					
R3	0.17	0.06				
T1	0.27	−0.20	−0.10			
T2	−0.16	0.37	−0.20	−0.54		
T3	−0.08	−0.14	0.35	−0.49	−0.44	
Q1	0.25	0.22	0.21	0.07	0.04	0.11

NO_3–AA	R1	R2	R3	R4	T1	T2	T3	T4	Q1
R2	−0.68								
R3	−0.65	0.27							
R4	−0.88	0.63	0.64						
T1	0.94	−0.63	−0.66	−0.86					
T2	−0.93	0.74	0.48	0.84	−0.93				
T3	−0.24	−0.14	0.49	0.24	−0.40	0.03			
T4	−0.04	−0.12	0.08	0.08	−0.15	−0.05	0.50		
Q1	0.19	−0.02	−0.16	−0.26	0.13	−0.16	0.04	0.18	
Q2	−0.26	0.19	0.14	0.34	−0.29	0.24	0.18	0.28	−0.11

NO_3–AA is also larger. The other bonds (R2 and R3) are slightly shorter in NO_3–AA than in NO_3, but equal to each other.

The bond angle T1 is larger in the presence of AA and, as a consequence of the flatness of the structures, the bond angles T2 and T3 are smaller. The spread in the bond angles T1 and T2 is significantly increased by atom AA, while the spread in T3 is smaller. From this we can conclude that bond R3, located opposite to the atom AA, shows more variation in direction than bond R2, although the bond lengths R2 and R3 are equal in both the NO_3 and the NO_3–AA fragments.

There are only small correlations between the structural parameters in the NO_3 fragments. The only large correlations are a consequence of the flatness of the fragment. In the NO_3–AA fragments, on the other hand, there are large correlations between the bond lengths and the opposing bond angles; Ri vs. Ti (Fig. 2(d–f)). The small spread in the bond angle T3 is responsible for the relatively small correlation between R3 and T3. The atom AA causes an increase in the correlation between T1 and T2, which shows again the flexibility of the geometrical parameters of atom O3 (direction of the bond R3). Correlations between R1 and R2 can be regarded as a result of correlations between bond lengths and angles. There are no direct relations between structural parameters and the dihedral angles Q1 and Q2.

Figure 2g shows three separate groups of bond length R4 (O–AA). The first group with values R4 $\sim$ 1.05 Å corresponds to AA = hydrogen atom, the second group with R4 $\sim$ 1.45 Å corresponds to AA = carbon atom and the third group with R4 > 1.90 Å corresponds to AA = metal atom. The scatter diagrams (Fig. 2(j,k)) show well defined regions for fragments with AA = C, while the metal bound fragments show a large range of values for R1, R4 and T4.

Figure 2(l) indicates that large values of Q2 (atom AA out of the plane of the fragment) occur for small R1 values with AA = metal atom. The structures with

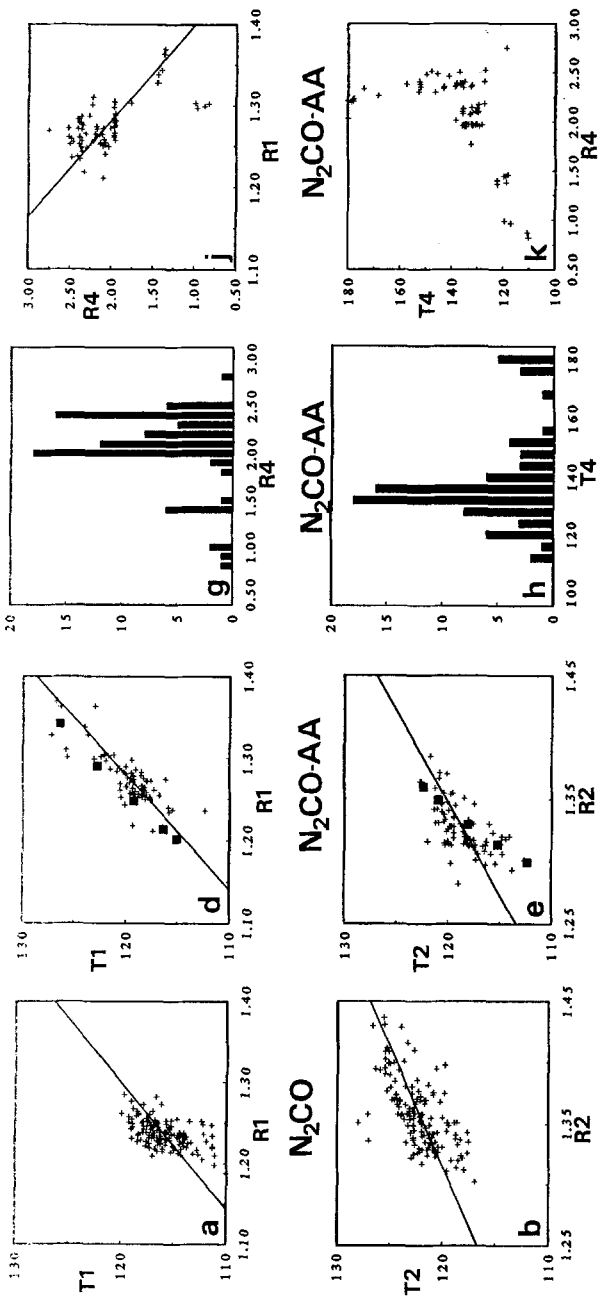

Fig. 3. Scatter diagrams and histograms of the N_2CO (*a–c*) and N_2CO–AA (*d–l*) fragments. Each *dot* represents a structure in the CSD. The *straight line* represents a least squares fit with the data from the CSD. The *solid squares* represent the *HF*/6-31G** calculations

AA = carbon atom have large R1 values and are lying in the plane of the fragment.

3.1.2 The N_2CO fragments. The same analysis, presented above for the nitrate fragments, are given in Tables 3 and 4 and in Figs. 3 and 4 for the fragments N_2CO and N_2CO–AA. We should remember that the number of N_2CO–AA

Table 3. Geometry of the N_2CO and N_2CO–AA fragments from the CSD

	N_2CO[a]		N_2CO–AA[b]	
	$\bar{x}$	σ_x	$\bar{x}$	σ_x
R1	1.237	0.017	1.275	0.030
R2 }	1.356[c]	0.028	1.328	0.020
R3 }			1.329	0.020
R4			2.064	0.395
T1	115.89	2.07	119.74	2.67
T2 }	122.05[c]	2.26	118.73	2.18
T3 }			121.49	1.54
T4			138.25	16.71
Q1[d]	0.03	0.75	0.38	1.30
Q2[d]			6.07	44.96

[a] The number of structures is 144
[b] The number of structures is 80
[c] Average values of the two indistinguishable bond lengths/angles
[d] Q1 and Q2 can be both positive and negative here

Table 4. Correlation matrices of the structural parameters of the N_2CO and N_2CO–AA fragments

N_2CO[a]	R1	R2	R3	T1	T2	T3
R2	−0.51					
R3	−0.38	−0.31				
T1	0.51	−0.27	−0.27			
T2	−0.23	0.63	−0.49	−0.42		
T3	−0.24	−0.36	0.72	−0.49	−0.58	
Q1	0.05	0.07	−0.02	−0.02	−0.02	0.03

N_2CO–AA	R1	R2	R3	R4	T1	T2	T3	T4	Q1
R2	−0.37								
R3	−0.40	0.14							
R4	−0.65	0.42	0.47						
T1	0.82	−0.33	−0.24	−0.58					
T2	−0.76	0.63	0.21	0.66	−0.81				
T3	−0.34	−0.32	0.12	0.07	−0.58	0.00			
T4	−0.42	0.45	0.29	0.50	−0.17	0.48	−0.39		
Q1	0.19	−0.12	−0.03	−0.16	0.22	−0.30	0.00	−0.13	
Q2	−0.06	0.30	0.17	0.30	0.10	0.26	−0.54	0.55	0.01

[a] 4-cyclic bond R1–T1 = 0.64, R2–T2 = 0.90, R3–T3 = 0.84
5-cyclic bond R1–T1 = 0.22, R2–T2 = 0.50, R3–T3 = 0.49
6-cyclic bond R1–T1 = 0.57, R2–T2 = 0.60, R3–T3 = 0.53

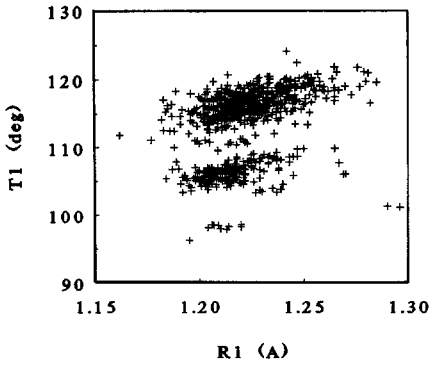

Fig. 4. Scatter diagram (R1 vs. T1) for all N_2CO fragments in the CSD

fragments without cyclic bonds is relatively small, which might influence the statistical analysis. Since many observations for the N_2CO–AA fragments are the same as for the NO_3–AA fragments, we will especially point out some differences.

The N_2CO fragment occurs often as part of a cyclic structure, connecting the two nitrogen atoms. We found 11 structures in the CSD with a cyclic bond of 4 atoms denoted by 4-N_2CO. The connecting atom is always found to be a phosphorus atom. In the 5 and 6 cyclic bonds (5-N_2CO and 6-N_2CO) the ring structure is formed by carbon and nitrogen atoms. There are hardly differences in the bond lengths (R1, R2 and R3) of the 4,5,6-cyclic structures. Obviously there are large differences in the bond angles. Figure 4, a scatter diagram R1 vs. T1, shows three separate groups. The bottom group consists of the 4-cyclic structures, the middle group the 5-cyclic and the top group incorporates both the 6-cyclic and the acyclic structures. All these groups show the same correlation between R1 and T1. The cyclic structures will further not be considered.

The bond length R1 (C=O) (Table 3) is slightly larger in N_2CO–AA than in N_2CO, while R2 and R3 (C–N) are smaller. Contrary to the observations in the NO_3 fragment, only the spread in bond length R1 becomes larger by the presence of atom AA.

The geometrical parameters of atom N2 are more flexible than those of atom N1 in the N_2CO fragment, the same as we found for the NO_3 fragment, only to a smaller extent. The fragment N_2CO is also found to be planar.

The correlation between R1 and T1 is significantly increased by the presence of the atom AA, while the correlation between R3 and T3 is much smaller in the N_2CO–AA fragments than in the N_2CO fragments. The correlations T1 vs. T2 and T1 vs. T3 are large for the N_2CO–AA fragments, the same as found for the NO_3–AA fragments.

Figure 3(g–l) shows the same groups for the bond lengths R4 as discussed for the NO_3 fragment. The spread in Q2 values is large for this fragment (Fig. 3i). Whether the atom AA is in or out of the plane of the fragment has no influence on the geometry of the fragment (Fig. 3(l)). The scatter diagram R4 vs. T4 (Fig. 3k), i.e. the position of atom AA relative to the fragment, shows a narrow band. The larger T4 values, corresponding to fragments connected to a metal atom, are found for large bond lengths R4 ($\sim$2.3 Å). For the smaller angles there is a linear dependence with R4, including structures with AA = metal atom, as well as AA = carbon atom.

3.2 Quantum chemical calculations

The analysis of the crystal structures, as discussed in the previous sections, showed correlations between bond lengths and angles. In this section we try to explain, on basis of Hartree–Fock calculations, the relations between the bond lengths Ri and angles Ti. Special attention will be paid to the different behaviour of the bond length R3 compared to R2 and to the position of the atom AA bonded to the oxygen atom.

3.2.1 Calculated molecular geometries. Several perturbations can cause the correlations between geometrical parameters as have been found in the CSD. There are also several ways to simulate these changes by HF calculations. Figure 5 shows the relation between R1 and T1 of the nitrate fragment, $NO_3^- - q$. The following conditions have been applied to the calculations to influence the structural parameters:

– Varying the magnitude of the point charge q and optimizing the total geometry.

– Varying the angle T4 and keeping the bond length R4 constant (= 0.96 Å), while optimizing the rest of the geometry.

– Varying the distance R4 from the point charge to the oxygen atom and keeping the angle T4 constant (= 108.00°), while optimizing the rest of the geometry.

– Varying the bond length R1 and optimizing the rest of the molecule, without the presence of a point charge.

There are two important features in Fig. 5. First, all the lines are pointing in the same direction: the bond angle T1 increases with increasing bond length R1. Second, the largest variation in T1 is caused by varying the magnitude of the point charge from $q = 0|e|$ to $1.4|e|$. This large variation in T1 agrees with the database results (Fig. 2d). This shows that correlations between structural parameters in the molecule can be studied by calculations using a point charge of varying magnitude, on which basis functions are centred.

We will now discuss the effect of a point charge on the geometry of the molecules. For all calculations we used a 6-31G** basis set. Applying a smaller 4-31G basis set yields the same results for the molecular geometries, but might give slightly inferior results for the density distributions. Tables 5 and 6 list the

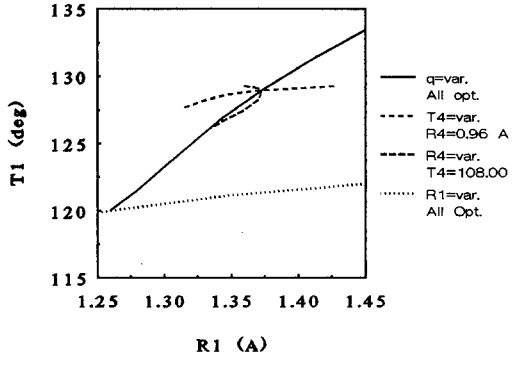

Fig. 5. Bond length R1 vs. bond angle T1 of the nitrate ion calculated with a 4-31G basis set

Table 5. Molecular geometry and properties at the critical points[a] of the nitrate ion. Hartree–Fock calculations using a 6-31G** basis set

Bond	q	R	$d(r_c)$	$\varrho(r_c)$	$\nabla^2\varrho(r_c)$	ε_π	T	α
R1	0.0	1.2259	0.604	0.513	−1.213	0.135	120.00	0.0
	0.2	1.2446	0.612	0.493	−1.154	0.141	121.54	0.2
	0.6	1.2853	0.622	0.451	−1.077	0.149	125.03	0.8
	1.0	1.3324	0.625	0.405	−0.963	0.148	129.11	1.5
	1.4	1.4092	0.637	0.333	−0.617	0.132	134.44	2.1
R2	0.0	1.2259	0.604	0.513	−1.213	0.135	120.00	0.0
	0.2	1.2172	0.600	0.523	−1.248	0.138	119.20	0.2
	0.6	1.2021	0.594	0.541	−1.294	0.141	117.29	0.7
	1.0	1.1881	0.589	0.557	−1.317	0.140	114.86	1.5
	1.4	1.1708	0.582	0.576	−1.348	0.129	111.43	2.4
R3	0.0	1.2259	0.604	0.513	−1.213	0.135	120.00	0.0
	0.2	1.2130	0.598	0.528	−1.268	0.140	119.26	0.2
	0.6	1.1905	0.587	0.555	−1.364	0.146	117.68	0.7
	1.0	1.1725	0.578	0.576	−1.425	0.146	116.03	1.4
	1.4	1.1550	0.570	0.597	−1.473	0.134	114.12	2.3
R4	0.0	—	—	—	—	—	—	
	0.2[b]	1.0963	—	—	—	—	106.74	
	0.6[b]	1.0029	—	—	—	—	106.86	
	1.0	0.9511	0.780	0.384	−2.659	0.033	105.41	
	1.4	0.9430	0.600	0.522	−2.290	0.105	103.81	

[a] Explanation of the symbols:
R: Bond length Ri (in Å) and corresponding bond angle Ti.
$d(r_c)$: Distance critical point (in Å) to central atoms (N).
$\varrho(r_c)$, $\nabla^2\varrho(r_c)$: Electron density (in a.u.) and Laplacian of ϱ at r_c.
ε_π: Π-character of ϱ at r_c. Ellipticity $\varepsilon_\pi = (\lambda_1/\lambda_1) - 1$, both curvatures are negative, while λ_2 is defined perpendicular to the molecular plane.
α: Bond path angle minus geometrical bond angle (in degrees). See Fig. 7
[b] No (3, −1) critical point present in the bond

bond lengths and angles of the molecules, while this information is also included in the scatter plots Figs. 2(d–f) and 3(d–f). The figures show a very good agreement between the calculated and observed structural parameters. A point charge varying from $q = 0|e|$ to $1.4|e|$ causes the same kind of variations in structural parameters, as different environments in crystal structures. The calculations show a smaller change in the bond angle T3 than in T2, in agreement with the CSD data and with the calculations reported by Del Bene and Radovick [13]. The calculated correlation between R2 and T2 in urea (Fig. 3e) shows a deviation from least-squares fit to the observed data, but the calculated values are in the proper range.

3.2.2 Electron density distributions. In this and the next section the changes in the electron density distribution caused by the point charge q will be discussed. Figure 6 shows the electron density redistribution in the nitrate ion caused by the presence of a point charge $q = 1.0|e|$. The electron redistribution in the molecular plane shows that the proton ($q = 1|e|$) attracts σ-electrons from the oxygen atom O1 and also from the rest of the molecule. Another large charge redistribu-

Table 6. Molecular geometry and critical point properties of urea. Hartree–Fock calculations using a 6-31G** basis set. For the definition of the symbols see Table 5

Bond	q	R	$d(r_c)$	$\varrho(r_c)$	$\nabla^2\varrho(r_c)$	ε_π	T	α
R1	0.0	1.2018	0.394	0.433	0.091	0.088	115.15	0.0
	0.2	1.2146	0.397	0.421	−0.023	0.066	116.40	0.5
	0.6	1.2479	0.405	0.390	−0.176	0.020	119.37	1.7
	1.0	1.2905	0.414	0.350	−0.211	−0.029	122.78	2.6
	1.4	1.3423	0.425	0.303	−0.115	−0.084	126.46	3.2
R2	0.0	1.3600	0.451	0.331	−0.981	0.049	122.42	−2.2
	0.2	1.3497	0.448	0.340	−1.013	0.057	121.04	−1.6
	0.6	1.3301	0.443	0.357	−1.081	0.086	118.18	−0.2
	1.0	1.3131	0.441	0.372	−1.159	0.138	115.28	1.2
	1.4	1.2995	0.441	0.385	−1.242	0.213	112.38	2.6
R3	0.0	1.3600	0.451	0.331	−0.981	0.049	122.42	−2.2
	0.2	1.3481	0.448	0.342	−1.037	0.066	122.56	−1.8
	0.6	1.3250	0.443	0.363	−1.131	0.107	122.46	−0.9
	1.0	1.3059	0.439	0.381	−1.210	0.166	121.95	0.2
	1.4	1.2915	0.438	0.394	−1.275	0.242	121.15	1.6
R4	0.0	—	—	—	—	—	—	
	0.2	1.1092	—	—	—	—	127.67	
	0.6	1.0058	—	—	—	—	121.25	
	1.0	0.9485	0.780	0.377	−2.645	0.016	116.58	
	1.4	0.9360	0.600	0.527	−2.389	0.065	112.65	

tion occurs in the plane perpendicular to the molecule at atom O1, where π-electrons accumulate. We will quantify this in the next section.

Tables 5 and 6 show besides the structural information, also topological properties of ϱ: the density ϱ, the Laplacian $\nabla^2\varrho$ and the ellipticity ε_π, at the (3, −1) critical point in the bond. The ellipticity ε_π is a measure for the π ($\varepsilon_\pi > 0$) or σ ($\varepsilon_\pi < 0$) character of the bond, as determined by the extent to which charge is preferentially accumulated in a given plane [24, 33]. We define it as $\varepsilon_\pi = (\lambda_1/\lambda_2) - 1$, where λ_1 and λ_2 are the negative curvatures of ϱ at the critical point and λ_2 refers to the direction perpendicular to the plane of the molecule. The ellipticity in the bonds in NO_3^-–q is hardly affected by the point charge q, which is remarkable with respect to the changes in atomic charges (see Sect. 3.2.3).

Upon increasing magnitude of q, the electron density decreases in the bond R1 and increases in R2 and R3. The Laplacian at the critical point agrees with this, since a decrease in $\nabla^2\varrho$ points to charge accumulation relative to the average of the density of the surrounding points.

For small values of q, no (3, −1) critical point is present in the bond O–q (R4); the electron density decreases continuously, starting from the oxygen atom in the direction of q.

The last columns in Tables 5 and 6 give information about the bond path angles. The bond path is the line of maximum electron density linking the nuclei [24]. The bond critical point is located at the position of lowest density on this line. A bond path will in general deviate from the geometrical bond which links

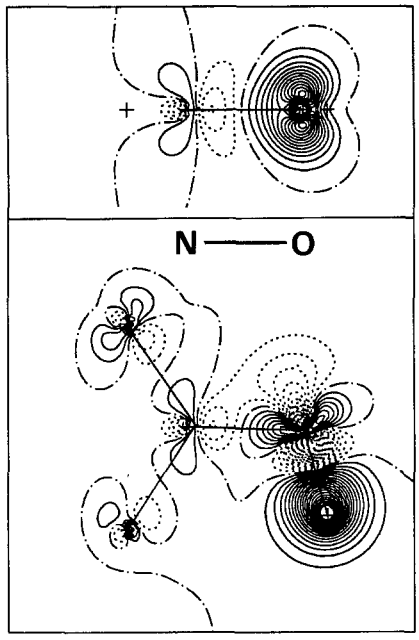

Fig. 6. Calculated (HF/6-31G**) electron rearrangement in the nitrate ion upon protonation: $\varrho(NO_3H)-\varrho(NO_3^-)$. The top figure shows the density in the plane perpendicular to the molecule, containing the N–O1 bond. The contour interval amounts to 0.1 e $Å^{-3}$

the nuclei by a straight line. Consequently the bond paths will make different angles, at the nuclear positions, than the geometrical bonds. The difference between the geometrical bond angle and the bond path angle (α_1, α_2, α_3), at the nuclear position, gives information about the deformation of the electron density of the molecular bond. A large value of α can be an indication that there is a force acting on the bond which causes a deformation of the electron density. For $q = 0$ the bond path angles at the central atom of the nitrate ion coincide with the geometrical bond angles, whereas in the urea molecule the bond paths in the C–N bonds are slightly drawn together. The behaviour of α_1, α_2 and α_3 upon protonation is the same for both molecules. The positive point charge q is seen to draw charge in its direction resulting in positive values for α_1 and α_2. The increase in the value α_3 (bond R3) can hardly be explained by the attraction of charge by q, because of the unfavourable direction of the bond R3 relative to the point charge. The deviation of the electron density distribution away from the geometrical bonds R2 and R3, as witnessed by the positive values of α_2 and α_3, can be used to explain the increase in the bond angle T1, upon increasing magnitude of q. With increasing values for α_2 and α_3, there is a driving force on the geometrical bonds R2 and R3 to follow the electron density distribution, resulting in an increase in bond angle T1. Wiberg and Laidig [34] have made the same observations in discussing the relation between electronegativity and bond path angles about sp^2 centres.

These topological analyses of the density do not show a clear difference between the bonds R2 and R3 and cannot explain the smaller variations found in the bond angle T3 than in T2. A direct interaction (steric hindrance) of the proton with atom O2 of the nitrate ion might restrict the variations in the angle T3.

3.2.3 Atomic charges. The atomic charges listed in Tables 7 and 8 have been calculated with Hirshfeld's charge partitioning method. The situation we study,

Table 7. Number of σ- and π-electrons and atomic charges of the nitrate ion according to the Hirshfeld partitioning method. The geometry of the molecules has been optimized with the HF method using a 6-31G** basis set

	q	N	O1	O2	O3	q
N(σ)	without q	5.466	6.845	6.845	6.845	—
	0.0	5.436	6.544	6.817	6.843	0.361
	0.2	5.432	6.529	6.811	6.833	0.397
	0.6	5.412	6.456	6.792	6.808	0.533
	1.0	5.382	6.399	6.761	6.775	0.685
	1.4	5.344	6.349	6.714	6.721	0.874
N(π)	without q	1.214	1.595	1.595	1.595	—
	0.0	1.204	1.536	1.589	1.594	0.075
	0.2	1.204	1.589	1.568	1.560	0.079
	0.6	1.207	1.672	1.528	1.494	0.099
	1.0	1.218	1.735	1.492	1.441	0.113
	1.4	1.228	1.787	1.461	1.405	0.118
Charge	without q	0.320	−0.440	−0.440	−0.440	—
	0.0	0.360	−0.080	−0.406	−0.437	−0.437
	0.2	0.365	−0.118	−0.379	−0.393	−0.276
	0.6	0.381	−0.128	−0.319	−0.302	−0.032
	1.0	0.400	−0.134	−0.255	−0.216	0.202
	1.4	0.428	−0.136	−0.175	−0.127	0.408

Table 8. Number of σ- and π-electrons and atomic charges of urea according to the Hirshfeld partitioning method. The geometry of the molecules has been optimized with the HF method using a 6-31G** basis set

	q	C	O	$N1H_2$	$N2H_2$	q
N(σ)	without q	4.759	6.900	7.171	7.171	—
	0.0	4.739	6.606	7.160	7.170	0.327
	0.2	4.735	6.603	7.148	7.154	0.361
	0.6	4.719	6.540	7.117	7.120	0.504
	1.0	4.697	6.473	7.086	7.087	0.659
	1.4	4.665	6.386	7.054	7.053	0.840
N(π)	without q	0.987	1.504	1.754	1.754	—
	0.0	0.980	1.452	1.751	1.753	0.063
	0.2	0.973	1.493	1.734	1.734	0.066
	0.6	0.959	1.572	1.693	1.687	0.088
	1.0	0.958	1.649	1.651	1.638	0.104
	1.4	0.969	1.717	1.611	1.591	0.111
Charge	without q	0.254	−0.404	0.075	0.075	—
	0.0	0.281	−0.057	0.090	0.077	−0.391
	0.2	0.293	−0.096	0.119	0.112	−0.227
	0.6	0.322	−0.112	0.190	0.193	0.008
	1.0	0.346	−0.122	0.263	0.276	0.297
	1.4	0.365	−0.106	0.336	0.356	0.449

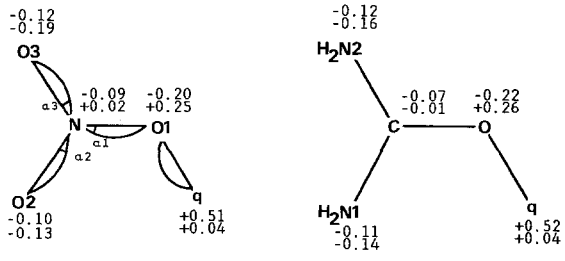

Fig. 7. Electron redistribution in the nitrate ion and urea molecule upon protonation ($q = 1.0|e|$). σ-electrons are given above, π-electrons below. The definition of the α's, i.e. the deviation of the bond path angles with the geometrical bond angles, is given

the addition of a point charge to a molecule, makes a charge partitioning in the neighbourhood of q difficult. Because of the absence, for small values of q, of a critical point in the bond R4, Bader's partitioning method will ascribe all charge close to q to another atom. We partly avoid this problem with Hirshfeld's method, by using the free atomic density of a hydrogen atom for the free atomic density of the point charge. Calculations with a point charge $q = 0$ show the problem of partitioning the density for our analysis. An extension of the number of nuclei over which the charge is divided, influences the analysis. To be able to compare the atomic charges of the nitrate ion with those of the urea molecule, the atomic charges of the amino group of urea are represented by a single value $q(NH_2)$.

From Tables 7 and 8 and from Fig. 7 it can be seen that both molecules show the same charge redistribution upon protonation. All atoms lose σ-electrons to the point charge, while the outer atoms/groups (O2 and O3 in NO_3^-, NH_2 in urea) donate π-electrons to the protonated oxygen atom (see also Refs. [11, 13]). The magnitude of the changes in the charge redistribution are almost equal for both molecules. Since the atoms constituting the molecules are different, the redistribution of charge must be a property which is determined mainly by the point charge. More detailed calculations show that the charge redistribution is mainly caused by the presence of the proton itself and only to a small extent by the resulting changes in molecular geometry. This is witnessed by very small changes in Hirshfeld atomic charges and figures of the electron density distribution, with different molecular geometries.

Besides the changes in the bond path angles, as discussed in the previous section, there is a second explanation for the increase in the bond angle T1 with increasing magnitude of q. As a consequence of the decrease of charge of the atoms/groups (O2 and O3 in NO_3^-, NH_2 in urea) they repel each other because of the smaller screening of the nuclei [13]. The angle T1 increases. The charge redistribution does not explain the shortening of the bonds R2 and R3 upon protonation. Because the groups lose charge they do not only repel each other but they would also be expected to repel the central atom (N for the nitrate ion and C for urea), increasing the bond lengths.

3.2.4 Electrostatic potential and Laplacian. In this section we will consider the position of the point charge relative to the molecule. It is well known that from the electrostatic potential $V(r)$ of a molecule, information can be obtained about interactions between molecules. A positive point charge is most likely to approach a molecule at the position of lowest electrostatic potential.

The valence shell electron pair repulsion model (VSEPR) of Gillespie [35] is very successful in predicting geometries of closed shell molecules. The model is based on two assumptions:

1. The charge density in the valence shell of an atom is spatially localized into pairs of electrons.

2. The geometrical arrangement of the electron pairs about an atom is that which maximizes the distance between the electron pairs.

These electron pairs can be located inside a bond, linking two atoms and can be non-bonded, representing the so called lone-pairs. Bader [31, 32] showed that the local charge concentrations in the electron density distribution around an atom, as defined by the Laplacian, can be identified with the hypothetical electron pairs of the VSEPR model. A local charge concentration in a non-bonded region, corresponding to a minimum in $\nabla^2\varrho(r)$, behaves similarly to a lone-pair in the VSEPR model. The position of this minimum is the most susceptible site of the molecule for electrophilic attack. From these observations it is clear that similar information, with respect to electrophilic and nucleophilic attack can be obtained from the Laplacian of ϱ and from the electrostatic potential. An advantage of the Laplacian over the potential is that it is a local property.

Figure 8 shows $V(r)$ and $\nabla^2\varrho(r)$ for the nitrate ion. The calculations have been performed on the free molecules; without a point charge. The bond length R1 has been varied (and kept fixed) while the rest of the geometry is optimized. Table 9 lists the characteristic information of $V(r)$ and $\nabla^2\varrho(r)$; the positions and magnitudes of the minimum values, which are indicated by arrows in Fig. 8. The angles α_V and α_L are defined (for the nitrate ion) as N–O1–$V_{\min}$ and N–O1–$(\nabla^2\varrho)_{\min}$, respectively, with similar definitions for the urea molecule.

The angle of electrophilic attack α_V, of the fully optimized nitrate ion and urea molecule, agrees well with the calculated angles T4 of the point charge for small values of q, as can be seen in Tables 5 and 6. For larger values of q the angle corresponding with the Laplacian (α_L) is closer to T4 than the angle corresponding with the potential (α_V). Bader [24, 31, 32] argues that the Laplacian of ϱ contains a total potential of which the electrostatic potential is only one component. The Laplacian would therefore give a better description of processes of nucleophilic and electrophilic attack than the electrostatic potential.

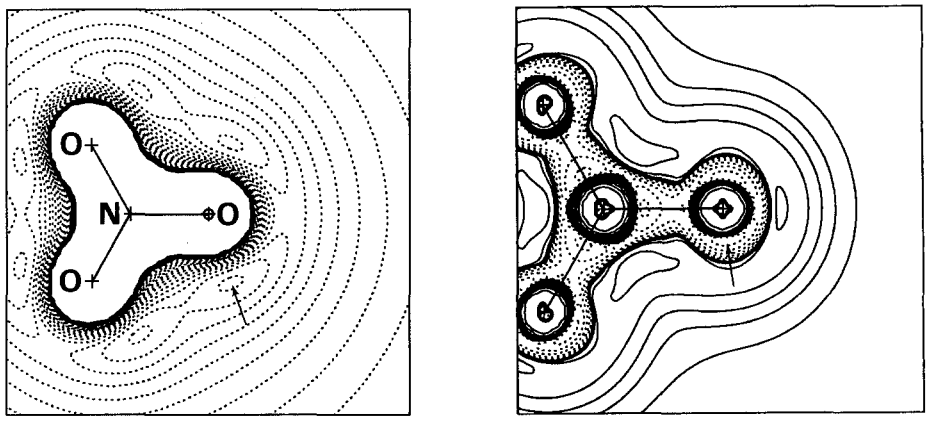

Fig. 8. Electrostatic potential (*left*) and Laplacian $\nabla^2\varrho(r)$ (*right*) of the nitrate ion. The contour interval for the potential amounts to 0.02 a.u. The contour intervals for the Laplacian increase by successive factors of 2 starting from 0.01 a.u. The *arrows* indicate the minima in the electrostatic potential and Laplacian

Table 9. Position[a] of electrophilic attack based on the electrostatic potential V and Laplacian $\nabla^2\varrho$. The geometry is optimized using HF/6-31G** keeping the bond length R1 fixed

R1	α_V	V_{min}	α_L	$(\nabla^2\varrho)_{min}$	λ_1	λ_2	λ_3
Nitrate							
1.10	110.22	−0.257	103.48	−6.924	−749.6	−30.7	−21.7
1.20	108.27	−0.280	100.94	−7.012	−747.6	−36.2	−18.1
1.30	105.21	−0.297	98.86	−7.076	−745.6	−41.3	−14.0
1.40	102.06	−0.309	97.16	−7.159	−747.1	−46.5	−10.1
1.2259[b]	107.26	−0.285	100.36	−7.029	−746.9	−37.5	−17.0
Urea							
1.10	142.43	−0.096	112.61	−5.682	−646.1	−12.2	−15.8
1.20	133.01	−0.113	106.39	−5.909	−657.5	−18.4	−14.7
1.30	125.72	−0.129	102.71	−6.107	−667.3	−24.5	−12.8
1.40	119.42	−0.141	100.10	−6.291	−677.0	−30.6	−10.3
1.2018[b]	132.83	−0.114	106.31	−5.912	−657.7	−18.5	−14.7

[a] Explanation of the symbols:
α_V: Angle (degrees) of approach (N–O1–V_{min}) based on the minimum in the potential V_{min}.
α_L: Angle (degrees) of approach based on the minimum in the Laplacian $(\nabla^2\varrho)_{min}$.
λ: Curvatures (in a.u.) of $\nabla^2\varrho$: λ_1 directed towards the oxygen atom.
λ_2 perpendicular to λ_1 and in the molecular plane.
λ_3 perpendicular to the molecular plane
[b] Optimized without constraint

We will now discuss the behaviour of the potential and Laplacian with changing bond length R1. The HF calculations showed with increasing magnitude of q an increase in bond length R1 and a decrease in the angle (R4) of electrophilic attack. We will discuss this in terms of V and $\nabla^2\varrho$. With increasing bond length R1, the minimum in the potential, V_{min}, decreases as well as the angle α_V. This is consistent with the behaviour of the position of the point charge. The angle α_V of electrophilic attack agrees with the calculations in the limit of $q \to 0$. The minimum in the Laplacian behaves the same as the potential, although the angle α_L is smaller than α_V.

The parameters λ in Table 9 are the curvatures (second derivatives) of the Laplacian and contain information about the shape of the area which is most susceptible for electrophilic attack. Regarding the behaviour of λ_2 and λ_3 (see Table 9 for the definitions) with increasing R1, the area of low $\nabla^2\varrho$ is extending in the direction perpendicular to the molecular plane, while it becomes smaller in the plane. This indicates that for larger bond lengths R1, it is easier for a point charge (atom) to be located out of the molecular plane, while at the same time the angle in the plane has less variation. This cannot be observed clearly in the crystallographic data, probably because of the limited number of observations.

4 Conclusions

From the analysis of the Cambridge structural database and the quantum chemical calculations of the protonation of the nitrate ion and urea molecule, we draw the following conclusions:

Protonation to an oxygen atom increases the bond length R1 of this atom as well as the angle T1 opposite to this bond. The direction of the bond R3, located trans to the proton, shows more variation than the bond R2, which is located cis to the proton. These observations have been made in the crystallographic data and are confirmed by the Hartree–Fock calculations.

The charge redistribution upon protonation is the same for the nitrate ion and the urea molecule. All atoms contribute σ-electrons to the proton, while π-electrons are transferred from the outer atoms to the protonated oxygen atom. This reduces the screening of the nuclei of the outer atoms/groups resulting in a repulsive force between these atoms/groups, which can explain the increase in the bond angle T1. Another explanation for the increased bond length T1 can be found in the changes in the bond path angles, upon increasing magnitude of point charge.

The properties of the electron density distribution at the critical points show no significant differences for the bonds R2 and R3. We have to consider that the critical points are not located in an area which is very sensitive for the forces on the nuclei, according to the electrostatic Hellmann–Feynman theorem.

The position of the point charge relative to the molecule can be understood by using both the electrostatic potential and the Laplacian of ϱ. The position of the point charge as calculated with the Hartree–Fock method agrees, for small values of q, with the position of the minimum of the electrostatic potential. For large values of q the Laplacian seems to give a better description of electrophilic attack. Increasing the magnitude of the point charge, the bond length R1 increases and the angle T4 decreases. This correlation can be understood by the changes in the potential and Laplacian of ϱ with increasing bond length R1 in the unprotonated molecules.

References

1. Dunitz JD (1979) X-Ray analysis and the structure of organic molecules. Cornell Univ Press, Ithaca
2. Bürgi HB, Dunitz JD (1983) Acc Chem Res 16:153
3. Allen FH, Kennard O, Taylor R (1983) Acc Chem Res 16:146
4. Nagy-Felsobuki EI von, Kimura K (1990) J Phys Chem 94:8041
5. Foucrault M, Hobza P, Sandorfy C (1987) J Mol Struct 152:231
6. Grein F (1988) Can J Chem 63:1988
7. Nguyen MT, Hegarty AF (1984) J Chem Soc Perkin Trans II 2037:2043
8. Umeyama H, Morokuma K (1976) J Am Chem Soc 98:4400
9. Del Bene JE, Vaccaro A (1976) J Am Chem Soc 98:7526
10. Del Bene JE (1977) J Am Chem Soc 99:3617
11. Del Bene JE (1978) J Am Chem Soc 100:1673
12. Del Bene JE (1978) Chem Phys Lett 55:235
13. Del Bene JE, Radovick S (1978) J Am Chem Soc 100:6936
14. Del Bene JE, Frisch MJ, Raghavachari K, Pople JA (1982) J Phys Chem 86:1529
15. Allen FH, Davies JE (1988) in: Isaacs NW, Taylor MR (eds) Crystallographic computing, vol 4, p 271. Oxford Univ Press, Oxford
16. Murray-Rust P, Motherwell WDS (1978) Acta Crystallogr B34:2534; Murray-Rust P, Raferty J (1985) J Mol Graphics 3:50; Murray-Rust P, Raferty J (1985) J Mol Graphics 3:60; CSD User Manual (1989) Cambridge Crystallographic Data Centre, Cambridge
17. Dupuis M, Spangler D, Wendoloski JJ (1980) NRCC Software Catalog, vol 1, Program N. QG01 (GAMESS); Guest MF, Kendrick J (1985) GAMESS Users Manual, Daresbury Laboratory

18. Dupuis M, Spangler D, Wendoloski JJ (1980) NRCC Software Catalog, vol 1, Program N. QG01 (GAMESS); Schmidt MW, Baldridge KK, Boatz JA, Jensen JH, Koseki S, Gordon MS, Nguyen KA, Windus TL, Elbert ST (1990) QPCE Bulletin 10:52–54
19. Hall GG (1985) Adv Atomic Mol Phys 20:41
20. Mulliken RS (1955) J Chem Phys 23:1833, 23:1841, 23:2338, 23:2343
21. Huzinaga S, Sakai Y, Miyoshi E, Narita S (1990) J Chem Phys 93:3319
22. Löwdin PO (1950) J Chem Phys 18:365
23. Hirshfeld FL (1977) Theor Chim Acta 44:129
24. Bader RFW (1990) Atoms in molecules – a quantum theory. Clarendon Press, Oxford
25. Bader RFW, Essén H (1984) J Chem Phys 80:1943
26. Biegler-König FW, Nguyen-Dang TT, Tal Y, Bader RFW, Duke AJ (1981) J Phys B14: 2739
27. Biegler-König FW, Bader RFW, Ting-Hua Tang (1982) J Comput Chem 3:317
28. Scrocco E, Tomasi J (1978) Adv Quantum Chem 11:116
29. Politzer P, Landry SJ, Warnheim T (1982) J Phys Chem 86:4767
30. Sjoberg P, Politzer P (1990) J Phys Chem 94:3959
31. Bader RFW, Chang C (1989) J Phys Chem 93:2946
32. Carrol MT, Cheeseman JR, Osman R, Weinstein H (1989) J Phys Chem 93:5120
33. Bader RFW, Slee TS, Cremer D, Kraka E (1983) J Am Chem Soc 105:5061
34. Wiberg KB, Laidig KE (1987) J Am Chem Soc 109:5935
35. Gillespie RJ (1972) Molecular geometry. Van Nostrand Reinhold, London